Contrib Mineral Petrol (1991) 106:325–339

Contributions to Mineralogy and Petrology

Trace elements (REE) and isotopes (O, C, Sr) to characterize the metasomatic fluid sources: evidence from the skarn deposit (Fe, W, Cu) of Traversella (Ivrea, Italy)

J. Vander Auwera * [1] **and L. Andre** [2]

[1] Laboratoire de Minéralogie et Géologie appliquée, Université Catholique de Louvain, B-1348 Louvain-La-Neuve, Belgium
[2] Laboratoires associés de Géologie, Pétrologie et Géochronologie, Université Libre de Bruxelles, B-1050 Bruxelles, Belgium

Received November 10, 1989 / Accepted July 24, 1990

Abstract. The skarn complex of Traversella was formed at the expense of various rock types (calcic hornfels, gneiss, dolomitic marble) occurring in the contact aureole of the dioritic intrusion of Traversella (30 ± 5 Ma). Application of phase equilibria has fixed the temperature of the primary stage of skarn formation between 550° C to 625° C. Similar applications indicate a larger range of temperature (525° C to 300° C) for the secondary stage. The different types of skarn (primary stage) are enriched in REE relative to the corresponding precursor rock (T.R. = 126 ppm (protolith) to 228 ppm (inner zone) for the skarn on gneisses; T.R. = 14 ppm to 71 ppm for the skarn on calcic hornfelses; T.R. = 12 ppm to 200 ppm for the skarn on dolomitic marbles), but all the inner zones of these different types of skarn show a similar REE distribution with a slight LREE fractionation and no Eu anomaly. It is inferred that the primary metasomatic fluid has a parallel REE pattern. The oxygen isotope composition of water in equilibrium with the early stage of skarn at $T = 600°$ C ranges from 8.3 per mil to 8.9 per mil. At the beginning of the first hydroxylation stage (secondary stage), the fluid $\delta^{18}O$ remains in the range observed in the primary stage but within it, there is a sharp decrease from 8.0 per mil to 5.0 per mil. During the sulphidation stage, the fluid $\delta^{18}O$ decreases more gradually from 5.0 per mil to 3.0 per mil. The I_{Sr} of the early skarn silicates ranges from the values observed in the dolomitic marbles (0.70874 to 0.70971) to the I_{Sr} of the intrusion (0.70947 to 0.71064). During the secondary stage, there is a progressive increase of the minerals I_{Sr} up to 0.71372. The REE pattern of the primary metasomatic fluid does not put any precise constraint on the primary fluid source. On the other hand, both stable and radiogenic isotopes suggest that the early high-temperature metasomatic fluid was isotopically equilibrated with the dioritic intrusion. This implies that this early fluid is either exsolved from the crystallizing intrusion or a metamorphic water previously equilibrated with the intrusion. During the secondary stage, the replacement of the early anhydrous phases by hydrated parageneses is accompanied by the mixing with meteoric fluid as indicated by stable ($\delta^{18}O$) and radiogenic ($^{87}Sr/^{86}Sr$) isotopes.

* *Present address*: Laboratoires associés de Géologie, Pétrologic, Géochimie, Université de Liège, B-4000 Sart Tilman, Belgium

Offprint requests to: J. Vander Auwera

Introduction

In the Traversella deposit (Ivrea, Italy), skarn masses were formed at the expense of several rock types: dolomitic marbles (exoskarns); calcic hornfelses; gneisses and the diorite itself (endoskarns). An iron-rich mineralization (magnetite) as well as traces of W (scheelite) are genetically linked to these skarns. The dioritic composition of the associated intrusion is a common feature of magnetite skarn deposits (Einaudi et al. 1981).

The formation of a typical skarn deposit which follows the contact metamorphism induced by the emplacement of the intrusion, is usually subdivided into a primary stage and a secondary stage (Burt 1972; 1977). During the primary stage, anhydrous minerals crystallize at the expense of the contact metamorphic parageneses. At lower temperature, in the secondary stage, hydrated phases and economic minerals are then formed at the expense of the early phases. These successive stages have been recognized in the Traversella deposit (Vander Auwera 1988) and the present study focuses mainly on defining the possible sources of the fluid(s) responsible for the two-stage evolution of these skarns. For this, several independent geochemical tracers have been selected: stable isotopes (C, O) and radiogenic isotopes (Sr), as well as REE.

Since natural waters of distinct origins differ in their isotopic signatures (Hoefs 1980; Taylor 1974), we have used stable isotopes (C, O) as discriminant parameters to trace the fluids. Calcite skarn is generally depleted in $\delta^{13}C$ and $\delta^{18}O$ in comparison with the isotopic composition of the marbles (Shieh and Taylor 1969; Taylor

and O'Neil 1977). This depletion can result either from the evolution of CO_2 during the decarbonation, or from the interaction with the infiltrating fluid (Bowman et al. 1985; Taylor and Bucher-Nurminen 1986; Guy et al. 1988). The isotopic data collected here put constraints on the respective role of these two processes and give information concerning the water-rock ratios which prevailed during the formation of skarns.

To our knowledge, the Sr isotopes have not yet been applied to a skarn system, although in hydrothermal deposits, these isotopes have made it possible to define the likely fluid sources (Norman and Landis 1983; Changkakoti et al. 1986; Bölkhe and Kistler 1986).

Complementary to this isotopic approach, the REE distribution will be used to trace the fluid sources, assuming that these elements were mobilized during the skarn formation.

Geological setting

The Traversella deposit was mined for its iron mineralization from the Roman period up to 1969. (Müller 1912; Colomba 1913; Kennedy 1931; Novarese 1943; van Marcke de Lummen and Vander Auwera 1990). It is located in the southern border of the Sesia-Lanzo zone (Italian Alps, Austro-alpine domain) (Fig. 1) which is essentially made up of pre-Alpine rocks submitted to Alpine tectono-metamorphic events. Two metamorphic episodes in the Alpine period have been recognized (Hunziker 1974): a high pressure phase (eo-Alpine metamorphism) observed in the southern part of the Sesia-Lanzo zone ("eclogitic mica schist" formation) and a low pressure phase in the northern part (eo-Alpine green schist facies: Sesia gneiss and Gneiss Minuti).

The Traversella pluton (Fig. 1) intruded the "eclogitic mica schist" formation during a late-magmatic event of the Alpine Orogenesis (Trumpy 1960; Debelmas and Lemoine 1970). This pluton has been dated at 30 ± 5 Ma; i.e., the Oligocene period (K-Ar method: Krummenacher and Evernden, 1960; radiation damage method: Chessex 1962). It is contemporaneous with the Biella and Adamello batholiths both located more to the East in the Austro-Alpine domain. The various rock types belonging to the "eclogitic mica schist" formation (mica schists, gneisses, dolomitic marbles, calcic hornfelses and eclogite lenses) form the surrounding rocks of the pluton. Major and trace elements modeling together with isotopic data have shown that this intrusion evolved through an assimilation fractional crystallization process (AFC) from dioritic to granitic composition (van Marcke de Lummen and Vander Auwera 1990).

Skarn lithology

The skarns are mainly located in the contact aureole [defined by the appearance of biotite at the expense of the regional metamorphic minerals such as glaucophane, garnet and phengite (Wirth 1985; 1986)] where they form massive bodies and veins. They develop either within the silica-aluminous (gneisses, diorite) and calcic rocks (dolomitic marble, calcic hornfels) or at the contacts between these rock types. These skarns display several features (pluri-decimetric size, dissymmetric pattern) which allow us to consider them as infiltration skarns (Korzhinskii 1970; Fonteilles 1978). They result from the interaction between an infiltrating fluid and a rock, initially in chemical disequilibrium. This interaction produces a typical geometrical pattern, which we have called a metasomatic column, characterized by a succession of zones of contrasting mineralogy, replacing each other across sharp or diffuse fronts (Korzhinskii 1970). The innermost zone which is located at the "source" of the fluid is the most affected by this interaction as the fluid flow proceeds from the inner towards the outer zones.

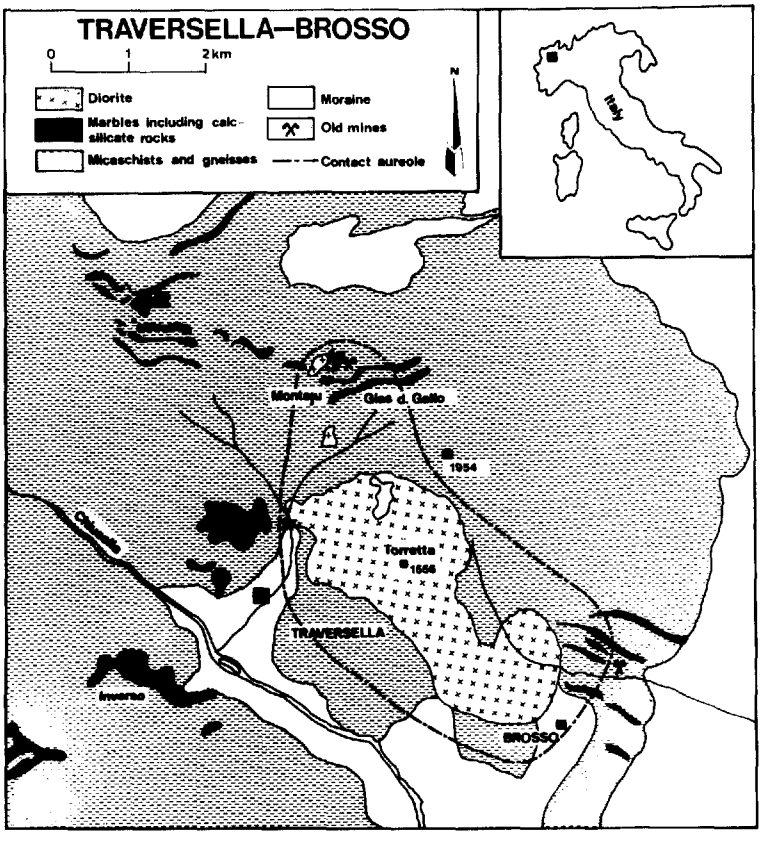

Fig. 1. Schematic geological map of the Traversella-Brosso area (after Müller 1912)

Table 1. Mineralogical composition of the different types of skarns (early stage)

Protolith	Metasomatic column (early stage)			
	Z1	Z2	Z3	Z4
Calcic hornfels (diopside-wollastonite ± garnet – ± feldspar)	Diopside	Salite andradite-rich garnet	/	/
Gneiss				
Biotite Oligoclase *K*-feldspar Quartz	Biotite oligoglase	Pyroxene andesine	Pyroxene bytownite	Garnet
Ilmenite Apatite, zircon	Ilmenite apatite, zircon	Sphene apatite, zircon	Sphene apatite, zircon	Sphene apatite, zircon
Dolomitic marble	Forsterite calcite	Pyroxene	Wollastonite	Quartz
Dolomitic marble	Forsterite calcite	Pyroxene	Andradite-rich garnet	
Dolomitic marble	Forsterite calcite ± spinel	Pyroxene	Grossular-rich garnet	

Skarns in diorite will not be considered here and have been described in another paper (Vander Auwera 1990).

Early stage

Depending on the lithology of the precursor rock (dolomitic marble, calcic hornfels, gneiss), different metasomatic columns have been recognized (see Table 1 for detailed mineralogical composition of the metasomatic columns). In the calcic hornfelses, the metasomatic column from the protolith to the innermost zone is: calcic hornfels / diopside / garnet whereas in the gneiss it is gneiss / pyroxene zone / garnet zone. In the case of the dolomitic marbles different types of metasomatic columns have been observed for the same protolith but the first two zones are always forsterite-calcite and diopside respectively with the innermost zone composed either of wollastonite or of garnet (andradite – rich or grossular-rich garnet). The feature common to all these metasomatic columns is the frequency of a garnet-rich zone in their inner part. The mineralogical variability of the internal zone of the skarns in dolomitic marbles is explained by variations in the chemical potentials of Al and Fe in the metasomatic fluid (Vander Auwera 1988).

The P–T conditions of this early stage have been estimated at 1 to 2 kb (stability of corundum in the presence of andalusite in the contact aureole of the intrusion, Si/Al ratio of the phengite) and 550° C to 625° C (X_{MgCO_3} of the primary skarn calcite; stability of calcite + forsterite ± spinel) (Vander Auwera 1988).

Secondary stage

Hydrothermal transformation, magnetite and scheelite deposition developed essentially in the skarns in dolomitic marbles and more precisely, in the forsterite-calcite zone while the other two zones were less affected (Dubru et al. 1988). Based on a detailed petrographic study, three main steps have been distinguished in the hydrothermal transformation of the forsterite-calcite zone (Fig. 2): two hydroxylation stages and one sulphidation stage, so defined as the former imply hydrated phases and the latter, sulphides. In the first hydroxylation stage, hydrated phases (talc, phlogopite) developed at the expense of forsterite and magnetite was precipitated,

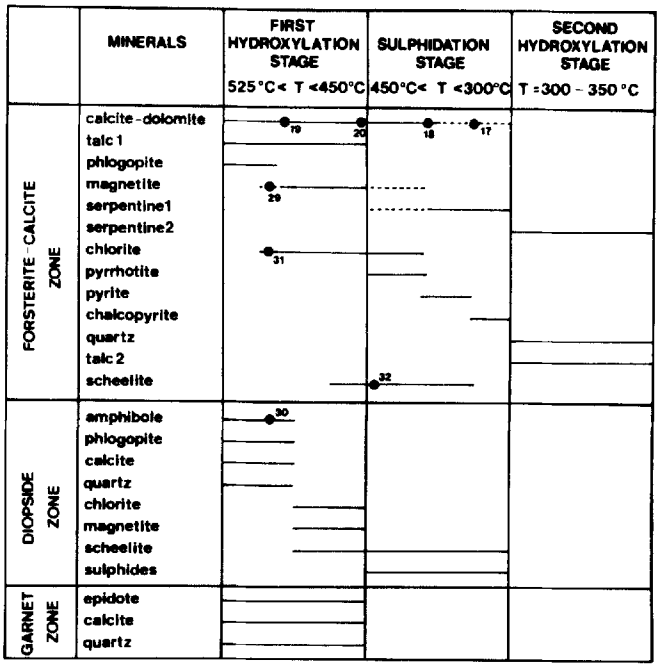

Fig. 2. Paragenetic table for the mineralization developed on the three zones of the skarns formed in dolomitic marbles at Traversella. The *points* indicate the relative position of the samples selected for the O–Sr isotopic study in the paragenetic sequence

together with part of the scheelite. The second stage (sulphidation stage) is characterized by the development of sulphides (mainly pyrite, pyrrhotite and chalcopyrite) and serpentine. During the third stage (second hydroxylation stage), massive talc or serpentine was formed.

It must also be emphasized that petrographic evidence indicates an overlapping development of magnetite and scheelite: the latter crystallized later than magnetite but its crystallization continued during the sulphidation of magnetite.

The temperature range of this secondary stage (525° C to 300° C) has been estimated using mineral parageneses and is relatively wide (Vander Auwera 1988): 525° C to 450° C for the first hydroxylation stage (based on the development of talc at the expense of forsterite and of tremolite at the expense of diopside); 450° C to 300° C for the sulphidation stage (based on the stability of serpentine and on the lack of monoclinic pyrrhotite); and approximately 300° C for the second hydroxylation stage. Though these temperature estimates are rather broad because of the small number of stable phases and the uncertainity in the evaluation of X_{CO_2}, this has little bearing on the interpretation (see later).

Analytical methods

Major elements were analysed by XRF (Université Catholique de Louvain). REE analyses by ICP were carried out in the spectrochemical laboratory of the Centre de Recherches Pétrographiques et géochimiques (CRPG) (analysed by Govindaraju) (Govindaraju and Mevelle 1987) on whole-rock samples (100 mg). Five REE-poor samples were analysed by INAA at the British Museum (Natural history (analysed by Williams). For each type of skarn, the analysed (REE) samples, representative of the different zones, were collected on the same outcrop.

Oxygen and carbon isotope determinations were performed at the Department of Geochemistry, Utrecht University (analysed by van Marcke de Lummen) using the method described by Nord and Billström (1982). The oxygen isotopic composition of silicates were determined at the BRGM (Fouillac analyst) (handpicked samples). For the two methods, an error of ± 0.2 per mil is estimated for $\delta^{18}O$ and $\delta^{13}C$ accounting for internal analytical precision.

The isotopic composition of Sr was determined on handpicked mineral samples (8 g). Sr was separated by conventional cation exchange techniques and its isotopic composition was measured by thermo-ionisation on double Re filaments on the Finnigan Mat 260 Spectrometer of the Belgian Centre for Geochronology. On the Mat 260 machine, the NBS 987 standard has a $^{87}Sr/^{86}Sr$ of $0.71024 + 0.00003$ ($2\sigma_m$) normalised to $^{88}Sr/^{86}Sr = 8.3752$.

Geochemical data

REE

The REE (Table 2) have been analysed in the various zones of the three types of skarns (early stage only: see Table 1): skarns in gneisses, skarns in dolomitic marbles and skarns in calcic hornfelses. In the case of the skarns on dolomitic marbles, only the metasomatic column with grossular-rich garnet in the internal zone has been considered (see Table 1). Separated pyroxene and garnet from the same garnet-pyroxenite of a skarn on calcic hornfels are also considered. In Fig. 3, the REE patterns of the original rocks (gneiss, dolomitic marble, calcic hornfels) (Fig. 3a) are compared to those of the innermost zone of the corresponding skarns (the most affected by the infiltrating fluid) (Fig. 3b). In the original rocks, the average absolute REE contents increase in the order: dolomitic marble (12 ppm or 4 ppm), calcic hornfels (14 ppm) and gneiss (126 ppm). There is a slight fractionation of the LREE relative to the HREE: $(La/Yb)_N = 9.3$ for the gneiss; 10.3 for the calcic hornfels; 7.0 or 4.0 for the dolomitic marbles and also a slight negative Eu anomaly. These REE patterns are similar or parallel to those observed for the North American Shale Composite (NASC) (Gromet et al. 1984).

The REE content in the skarns is clearly higher than that observed in the original rocks (Fig. 3b) especially when the substrate is a dolomitic marble or a calcic hornfels. For example, in the skarns in calcic hornfels, the total REE varies from 14 ppm in the precursor rock to 71 ppm in the garnet-pyroxenite. There is also, in the skarns, a slight modification of the $(La/Yb)_N$ ratio (an increase for the skarn in dolomitic marbles and in gneisses and a decrease for that in calcic hornfelses) and a lessening of the Eu anomaly compared to those observed in the corresponding original rocks. Moreover, the most striking feature is that, whatever the REE pattern observed in the original rock, the patterns of the skarns are very similar but with different total REE content. This is also observed in pyroxene and garnet belonging to the same garnet-pyroxenite (Fig. 3c): both minerals are characterized by a similar fractionation of the LREE and no observable Eu anomaly.

Table 2. REE data for the Traversella skarns and intrusion (CH: calcic hornfels; DM: dolomitic marble; G: gneiss; CPX: clinopyroxene; GRT: garnet)

	1 Dolomitic marble	2 Dolomitic marble	3 Calcic hornfels	4 Gneiss	5 Garnet pyroxenite CH	6 Garnet pyroxenite CH	7 Garnet pyroxenite DM	8 Garnet pyroxenite G	9 Granite	10 Diorite	11 Diorite	12 CPX CH	13 GRT CH
La	1.20	2.80	4.40	26.87	8.92	4.48	49.41	68.52	130.29	81.81	53.08	1.70	7.90
Ce	2.70	6.20	5.40	52.53	35.93	25.70	107.58	94.76	157.23	204.63	109.66	2.70	33.80
Nd	<1.00	2.20	2.50	27.16	16.27	21.54	29.38	37.42	43.22	123.47	50.45	<1.00	18.10
Sm	0.24	0.57	0.53	5.74	2.90	3.83	4.89	7.98	5.56	23.80	9.35	0.12	2.50
Eu	0.06	0.14	0.14	1.17	1.11	1.28	1.47	2.28	0.63	4.34	2.03	0.03	0.81
Gd	<0.50	<0.50	<0.50	4.78	2.20	2.49	3.76	6.57	4.14	16.73	7.21	<1.00	<2.00
Tb	0.03	0.06	0.09	–	–	–	–	–	–	–	–	<0.03	0.27
Dy	–	–	–	3.78	1.74	2.35	3.80	4.92	1.44	11.96	4.69	–	–
Ho	<0.02	<0.02	<0.02	–	–	–	–	–	–	–	–	<0.10	0.30
Er	–	–	–	1.97	1.04	1.44	2.24	2.49	0.78	5.68	2.41	–	–
Tm	<0.02	0.04	0.06	–	–	–	–	–	–	–	–	<0.05	0.19
Yb	0.19	0.26	0.28	1.94	1.00	1.47	2.22	2.33	0.77	5.12	2.49	<0.05	1.07
Lu	0.02	0.04	0.05	0.30	0.13	0.23	0.21	0.34	0.19	0.72	0.42	<0.02	0.20
Y	–	–	–	23.04	16.21	20.32	27.17	29.33	–	68.67	–	–	–

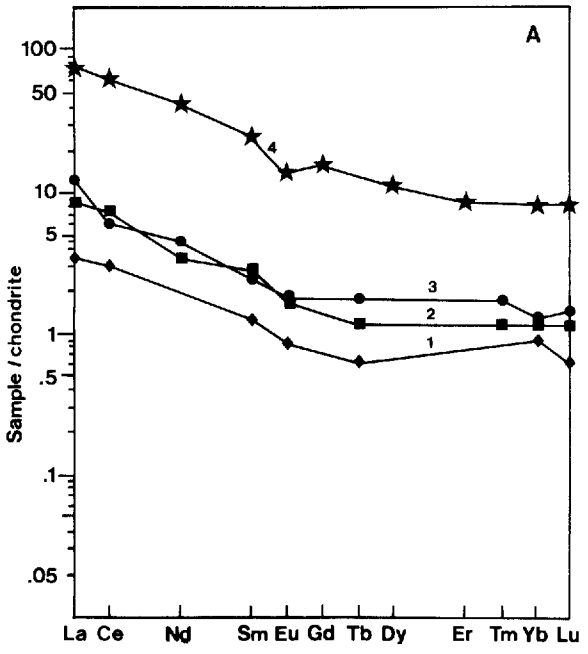

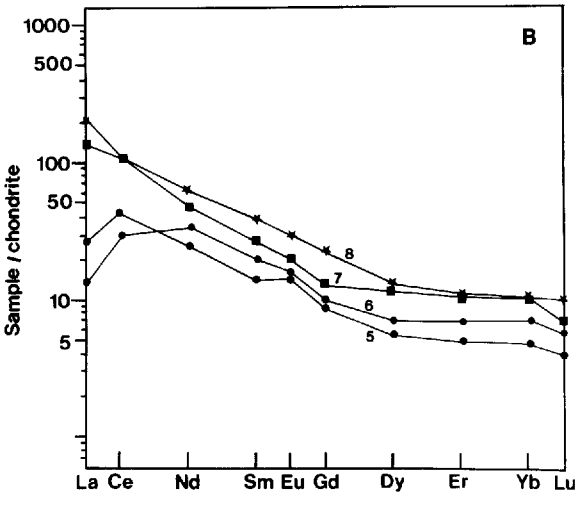

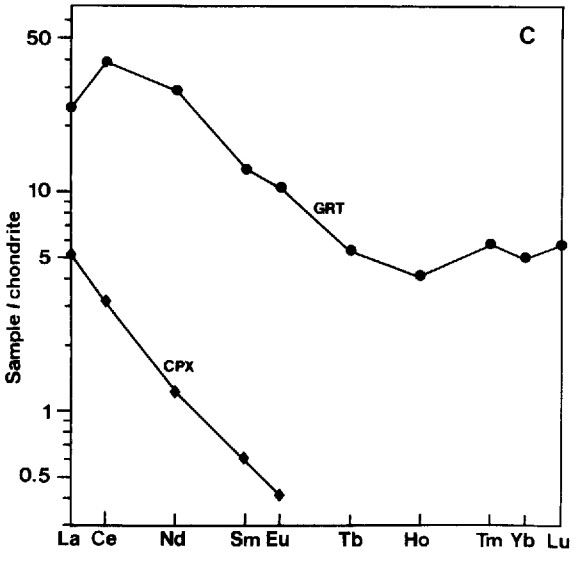

C, O isotopes

The data are presented in the $\delta^{18}O-\delta^{13}C$ diagram of Fig. 4 (see also Table 3). The sampling focused essentially on the skarns developed in dolomitic marbles with:

1. Four unmodified dolomitic marbles located outside the contact aureole (nos. 1–4 on Fig. 4) and eight modified dolomitic marbles located inside the contact aureole (nos. 5–13 on Fig. 4) (the data on Fig. 4 concern the calcitic fraction of these marbles).
2. Three primary calcites from forsterite-calcite zones, two of them (nos. 14, 15 on Fig. 4) from the metasomatic wollastonite column and one, from the metasomatic andradite column (nos 16 on Fig. 4).
3. Two silicates: a diopside from a skarn on dolomitic marble and a garnet from a skarn on calcic hornfels.
4. minerals belonging to the hydrothermal parageneses: samples of amphibole, chlorite, magnetite, scheelite, calcite and dolomite from the first hydroxylation stage and samples of calcite and dolomite from the sulphidation stage (Fig. 2 – Table 3).

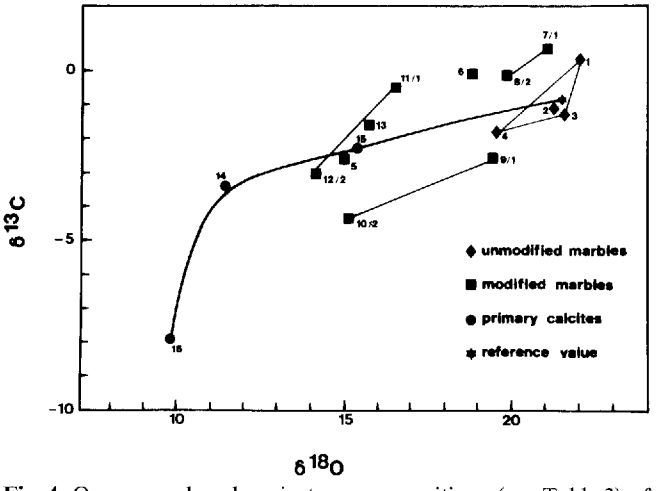

Fig. 4. Oxygen and carbon isotope compositions (see Table 3) of (1) primary calcites (*solid circles*) developed in the early stage of skarn development (forsterite-calcite zone: no. 14 and no. 15 belong to a metasomatic wollastonite column whereas no. 16 belongs to a metasomatic garnet column); (2) calcitic fractions of the dolomitic marbles located outside the contact aureole (Inverso) (unmodified marbles; nos. 1 to 4, *solid diamonds*); (3) the modified dolomitic marbles (*solid squares* nos. 5 to 13) located inside the contact aureole in proximity of the skarns. Among the latter samples, pairs of dolomitic marble (*tie lines*) located immediately at the contact with the first zone of the skarn (no. 2) and the less modified marble located at a few tens of cm further from the skarn (no. 1) have been distinguished (samples 5, 6 and 13 have been collected at a few cm of the skarn). The reference value (*solid star*) has been fixed at $\delta^{18}O = +21.6$ per mil and $\delta^{13}C = -0.93$ per mil (see text)

Fig. 3. **A** REE patterns of the different original rocks. ◆, ■: Dolomitic marbles; ●: calcic hornfels; ⋆: gneiss. **B** REE patterns of the internal zones of the corresponding skarns (*same symbols* as in **A**; *sample numbers* from Table 2). **C** REE patterns of cpx and garnet from the same garnet-pyroxenite of a skarn on calcic hornfels

Carbonates corresponding to the two different stages have been distinguished on the basis of the associated minerals of their paragenesis. The second hydroxylation stage has not been documented because of the lack of adequate mineral samples.

Early stage. There is a general trend towards a gradual decrease of the $\delta^{18}O-\delta^{13}C$ values from the marbles located outside the contact aureole to the primary calcites of the skarns, with intermediate values for the dolomitic marbles immediately adjacent to the first zone of the skarn. It is worth mentioning the scattered character of the isotopic composition of the modified marbles. The primary calcites of the skarn have the lowest $\delta^{18}O$ and $\delta^{13}C$, the calcites of the metasomatic wollastonite column (no. 16, Fig. 4).

Secondary stage. The isotopic composition of the minerals belonging to the secondary stage of skarn development is presented in Table 3.

Table 3. Stable isotopes data of skarn and dioritic samples DM/OCA, dolomitic marble outside the contact aureole; DM/ICA, dolomitic marble inside the contact aureole; CC/WC: calcite of the wollastonite column; CC/GC, calcite of the garnet column; CC II, calcite of the secondary stage; DOL II, dolomite of the secondary stage; D, diorite

Sample no.	Description	$\delta^{13}C_{PDB}$ (per mil)	$\delta^{18}O_{smow}$ (per mil)
A Carbonate and calcic fraction of the dolomitic marbles			
1	DM/OCA	+0.4	+22.0
2	DM/OCA	−1.1	+21.2
3	DM/OCA	−1.2	+21.5
4	DM/OCA	−1.8	+19.4
5	DM/ICA	−2.6	+14.9
6	DM/ICA	+0.03	+18.8
7	DM/ICA	+0.7[a]	+21.1[a]
8	DM/ICA	−0.1[a]	+19.8[a]
9	DM/ICA	−2.5[a]	+19.4[a]
10	DM/ICA	−4.3[a]	+15.2[a]
11	DM/ICA	−0.5	+16.5
12	DM/ICA	−3.0[a]	+14.1[a]
13	DM/ICA	−1.5[a]	+15.7[a]
14	CC/WC	−3.4	+11.4
15	CC/WC	−2.3	+15.33
16	CC/GC	−7.9[a]	+ 9.7[a]
17	CC II	−8.0	+ 8.6
18	DOL II	−6.4[a]	+12.8[a]
19	CC II	−7.7[a]	+ 8.7[a]
20	DOL II	−7.6[a]	+10.8[a]
B Dolomitic fraction of the dolomitic marbles			
21	DM/OCA	+0.7	+21.9
22	DM/OCA	−1.4	+21.6
23	DM/ICA	−2.1	+21.0
24	DM/ICA	−3.2	+18.2
25	DM/ICA	−0.1	+17.5
26	DM/ICA	−0.4	+16.6
C Skarn silicates (primary and secondary stages)			
27	Diopside	/	+ 7.2
28	Garnet	/	+ 5.4
29	Magnetite	/	+ 1.3
30	Amphibole	/	+ 6.3
31	Chlorite	/	+ 7.7
32	Scheelite	/	+ 3.3
D Intrusion whole rock (data from van Marcke de Lummen and Vander Auwera 1990)			
33	D	/	+ 7.7
34	D	/	+ 8.4

[a] Mean value of two analyses

Sr isotopes

To use Sr isotopes as tracers it is necessary to determine the Sr isotopic composition of the different materials at the time of the skarn development (30 ± 5 Ma) (=initial Sr isotopic ratio $=I_{Sr}$). Thus to minimize the error due to calculation of this initial isotopic ratio, Rb-poor minerals were selected: garnet and diopside from the skarn developed on calcic hornfelses; calcite and wollastonite from the skarn on dolomitic marbles; calcite and dolomite from the first hydroxylation stage and the sulphidation stage and lastly scheelite. The results of mineral analyses are shown in Table 4 together with values obtained for two dolomitic marbles and also for the intrusion. The epidote observed in some transformed facies of the intrusion has also been considered.

Early stage. The I_{Sr} of the different materials has been plotted on Fig. 5. In the intrusion, the ratios for the fresh samples and also two slightly altered samples (nos. 33, 34 on Fig. 5) range from 0.70947 to 0.71064. Samples nos. 33 and 34 fall respectively within the range of the

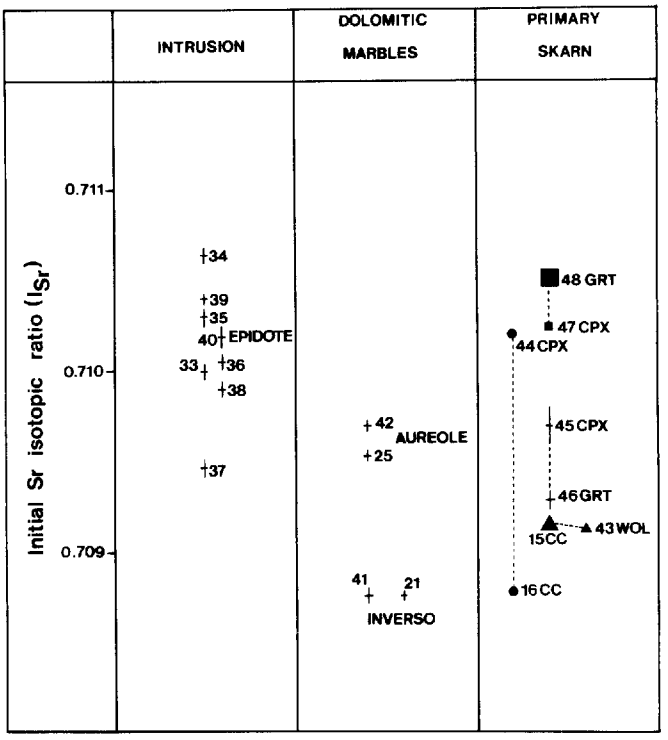

Fig. 5. Initial Sr isotopic ratio (I_{Sr}) (see Table 4). Minerals belonging to the same type of skarn have the same symbol (see text). *Variable dimensions* of *symbols* are for analytical error

Table 4. Sr isotopic composition of dioritic and skarn samples (primary and secondary stages). The initial Sr isotopic data has been calculated back to the maximum age of the intrusion (35 Ma: Krummenacher and Evernden 1960; Chessex 1962)

Sample no.	Description	Rb (ppm)	Sr (ppm)	$^{87}Rb/^{86}Sr$	$^{87}Sr/^{86}Sr$	$(^{87}Sr/^{86}Sr)$ 35 M.a.
A Dioritic rocks						
33	D	102	722	0.409	0.71020	0.71000
34	D	132	719	0.531	0.71090	0.71064
35	D	201	852	0.683	0.71064	0.71030
36	D	111	694	0.463	0.71028	0.71005
37	D	96	734	0.378	0.70966	0.70947
38	D	111	815	0.394	0.71010	0.70990
39	D	91.7	728	0.365	0.71059	0.71041
40	D (epidote)	0.5	264	0.005	0.71020	0.71020
B Dolomitic marbles						
21	OCA	2	122	0.045	0.70876	0.70874
41	OCA	0	187	0.000	0.70876	0.70876
42	ICA	0	234	0.000	0.70971	0.70971
25	ICA	0	406	0.000	0.70953	0.70953
Skarn minerals of the early stage						
16	SDM/GC/CC	11.5	743	0.045	0.70880	0.70878
15	SDM/WC/CC	4.7	327	0.042	0.70918	0.70916
43	SDM/W	0	318	0.000	0.70915	0.70915
44	SDM/GC/CPX	<2	31.1	<0.186	0.71030	0.71021
45	SCH/CPX	<2	17.1	<0.339	0.70988	0.70971
46	SCH/GRT	<2	13.6	<0.426	0.70950	0.70929
47	SG/CPX	81	751	0.313	0.71040	0.71024
48	SG/GRT	30.1	20.9	4.169	0.71259	0.71052
D Skarn minerals of the first hydroxylation stage						
20	DOL	1.2	69.8	0.050	0.71028	0.71026
19	CC	1.3	146	0.026	0.71030	0.71029
32	SCH	6.8	66.3	0.297	0.71092	0.71077
E Skarn minerals of the sulphidation stage						
18	DOL	0	202	0.000	0.71303	0.71303
17	CC	4.8	535	0.026	0.71373	0.71372

D, Diorite; OCA, outside the contact aureole; ICA, inside the contact aureole; SDM, skarn on dolomitic marble; SCH, skarn on calcic hornfels; SG, skarn on gneiss; GC, garnet column; WC, wollastonite column; CC, calcite; W, wollastonite; CPX, pyroxene; GRT, garnet; DOL, dolomite; SCH, scheelite

fresh samples or slightly above. The ratio for an epidote (no. 40 on Fig. 5) is in the same range (0.71020) as that of the intrusion.

In order to determine the Sr isotopic composition of the original surrounding dolomitic marbles, two groups of dolomitic marbles were analysed: one from the contact aureole (samples nos. 42, 25 on Fig. 5) and the other from Inverso (samples nos. 21, 41, Fig. 5) (Fig. 1). The values are very close in each group, although there is a large isotopic difference between the two groups. This feature is also observed for $\delta^{18}O$. Indeed, the marbles outside the aureole have $\delta^{18}O$ of about +22 per mil and the others, of about +16 per mil (see earlier).

For the minerals of the primary skarns, Fig. 5 illustrates three features:

1. The I_{Sr} is sometimes identical, sometimes strongly contrasted for minerals belonging to the same type of skarn. The former case is illustrated by the clinopyroxene and garnet from skarns in gneisses (filled squares), in calcic hornfelses (crosses) and the calcite and wollastonite from the skarns in dolomitic marbles (filled triangles). The latter case is shown by calcite and clinopyroxene from the skarns in dolomitic marbles (metasomatic column with garnet (filled circles, see earlier): the calcite (first zone of the skarn) has an I_{Sr} of 0.70878 while the clinopyroxene (internal part of the skarn), has an I_{Sr} of 0.71021. The distinct I_{Sr} of the minerals of the two types of metasomatic columns developed on dolomitic marbles (metasomatic columns with wollastonite or garnet) is correlated with the bulk Sr content. In the metasomatic wollastonite column, the Sr content of the minerals remains relatively constant (dolomitic marble: 246 ppm; calcite: 327 ppm; clinopyroxene: 209 ppm; wollastonite: 318 ppm) whereas in the metasomatic garnet column, the pyroxene from the internal part of the column is strongly Sr-depleted (dolomitic marble: 429 ppm; calcite: 743 ppm; pyroxene: 31 ppm).
2. The Sr isotopic composition is highly variable from skarn to skarn: 0.70878 to 0.71052 and this range covers those in the dolomitic marbles and the intrusion.

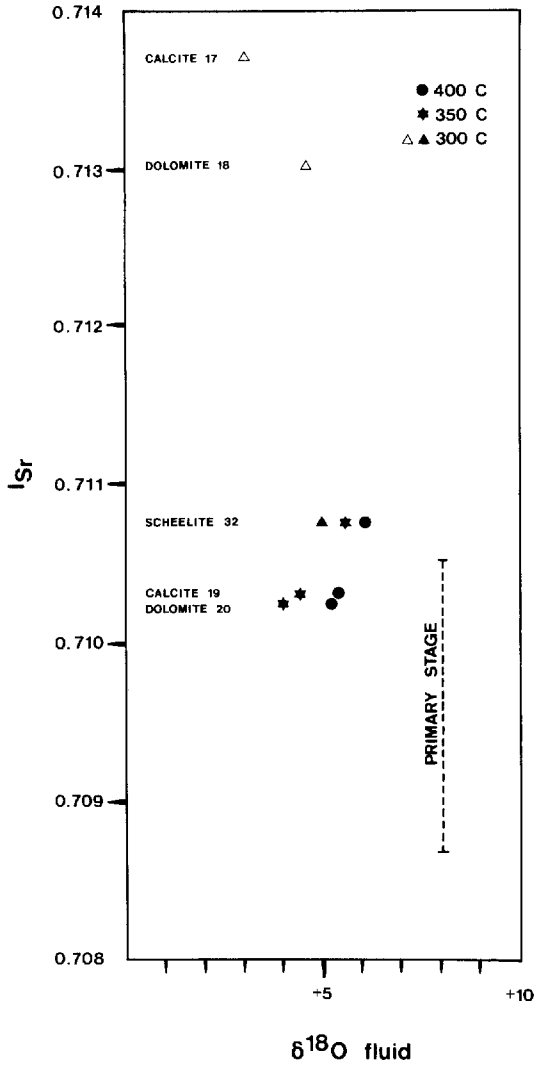

Fig. 6. Oxygen isotopic composition versus I_{Sr} of the fluid in equilibrium with the minerals representative of the secondary stage. *Solid symbols:* first hydroxylation stage; *open symbols:* sulphidation stage. The range in I_{Sr} obtained for the primary stage of skarn development has been plotted for comparison (see Fig. 5)

Table 5. Specific gravities and composition (in weight percent) of the different skarns. Specific gravities have been measured on a Berman balance

	CaO	TiO_2	Al_2O_3	g
Gneiss	–	–	15.37	3.11
Garnet zone on gneiss	–	–	15.40	3.18
Calcic hornfels	–	0.14	–	3.13
Garnet zone on calcic hornfels	–	0.13	–	3.48
Dolomitic marble	34.29	–	–	2.80
Garnet zone on dolomitic marble	29.79	–	–	3.39

3. The three clinopyroxenes are very similar but have distinct Sr contents.

Secondary stage. During the secondary stage (Fig. 6), there is a progressive increase of the minerals I_{Sr} up to 0.71372. The I_{Sr} of the phases corresponding to the first hydroxylation stage (0.71026 to 0.71077) is similar to that observed for both the primary skarn minerals and the intrusion, whereas in the sulphidation stage (up to 0.71372) the I_{Sr} is much greater. Moreover, this increase of the I_{Sr} is associated with a decrease in the fluid $\delta^{18}O$ (see later).

Discussion

Source of the primary metasomatic fluid

REE evidence

The clear increase in REE content from about 10 ppm (ΣREE) up to 200 ppm (ΣREE) in the inner zone of the skarn in dolomitic marbles for example can result either from a volume decrease, or from an input of these elements during the skarn formation process. An estimation of the volume variation implied by the development of the different types of skarns can be made with the help of the Gresens equation (Gresens 1967) which relates composition and volume variation during skarn formation.

$$100\left(f_v \frac{g_B}{g_A} c_B^n - c_A^n\right) = x^n$$

where f_v is the volume factor ($V_B = f_v \cdot V_A$ with V_A and V_B for the volume of rocks A and B); g_A and g_B are the specific gravities of A ans B; C_A^n and C_B^n, the weight fraction of component n in A and B and finally, X^n is the variation of component n during the transformation of rock A into B.

An evaluation of the f_v factor can be made if the perfectly inert behaviour of one component (i.e., an element which has not been affected by the metasomatism i.e., $x_n = 0$ (Fonteilles 1978)) can be demonstrated.

In the skarn on gneisses, Al_2O_3 can be considered as a perfectly inert component (Vander Auwera 1988) because the Al/Ti ratio remains constant throughout the column. According to the measured specific gravities and concentrations in the gneiss and garnet-pyroxenite zone (see Table 5), the f_v factor equals 0.98. In the skarn in calcic hornfelses, TiO_2 is not affected by the transformation of the calcic hornfels into a garnet-pyroxenite as the Ca/Ti ratio is relatively constant in this column. With this constraint the *fv* factor equals 1.00. In the skarn in dolomitic marble, $X_{Ca_0} = 0$ and f_v equals 0.95. Consequently, the volume variation seems to be negligible in the skarns considered here and the skarns' REE patterns are then thought to result from a strong input of these elements during skarn formation.

The similar REE patterns of the skarn internal zones (see earlier sec.) suggest that the different types of skarns result from interaction of the various rock types with the same fluid which has imposed its own pattern. This

last feature can also be deduced from the REE patterns of clinopyroxene and garnet of the same garnet-pyroxenite (Fig. 3C). Indeed the similar REE patterns preclude any equilibrium between the fluid and the two minerals because, if it were the case, a quite different REE distribution between clinopyroxene and garnet would be expected, in response to the different REE distribution factors (K_D) of these minerals (Henderson 1984; Cullers et al. 1973; Henderson, personal communication). This last obervation suggests further, that in the case of trace elements the metasomatic column cannot be considered as an ideal chromatographic column (i.e., in which the distribution of elements is controlled only by local equilibrium (Hofmann 1972)), because precipitation and adsorption processes can occur. From the preceding discussion, the REE distribution in the primary fluid can be estimated as parallel that of the internal zones of the skarns, i.e., with a LREE fractionation and no observable anomaly in Eu and Ce.

There are three possible sources for this primary metasomatic fluid: a fluid exsolved from the crystallizing intrusion, a metamorphic fluid and a meteoric fluid. As a consequence of fluid circulation, the fluid REE distribution may be affected. Nevertheless, as fluid circulation is a random process, we may expect to observe variable patterns depending on the position of the samples and this is not the case. So, in order to model the process, we can assume that the fluid was characterized by the same REE pattern it had at its source.

Using data from Flynn and Burnham (1978), on the partitioning of REE between a fluid and a crystallizing magma, it is now possible to assess the REE pattern of the fluid in equilibrium with the different rock types of the intrusion. We have considered here the K_D obtained at $P=1.25$ kb and $T=800°$ C as these conditions are possible for the Traversella intrusion (see earlier). Nevertheless, this approach is semiquantitative as the K_D also depends on the chlorine molality of the fluid, the P_{H_2O} and the magma composition (Flynn and Burnham 1978). These factors are difficult to constrain in the Traversella ore bodies and are particularly important for the Eu anomaly. The selected samples correspond to dioritic and granitic facies of the intrusion which have been demonstrated to be successive residual liquids (van Marcke de Lummen and Vander Auwera 1990). Comparison of these different calculated REE patterns (Fig. 7), with that of the metasomatic fluid shows that the best fit is obtained for the fluid in equilibrium with the diorites. Both distributions show similar $(La/Sm)_N$ but the metasomatic fluid has a slightly lower $(Gd/Yb)_N$.

A metamorphic fluid in equilibrium with the biotite-rich gneisses (the most abundant rocks of the contact aureole), should have a REE pattern parallel to that of North American Shale Composite (NASC) (Fourcade 1981) (Fig. 7). Here too, both metamorphic and metasomatic fluids have comparable $(La/Sm)_N$ but the $(Gd/Yb)_N$ is slightly higher in the metasomatic fluid. This is also true for a meteoric source, as the meteoric fluids are also characterized by a REE pattern close to that of NASC (Martin et al. 1976). Judging from the comparable REE patterns of these different fluids (metamorphic, metasomatic and in equilibrium with the diorite), the REE geochemistry alone cannot discriminate between the various sources.

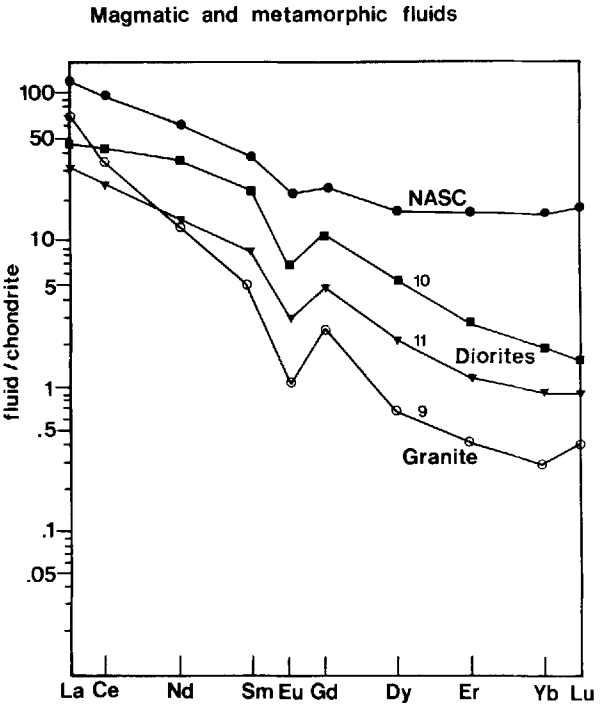

Fig. 7. Calculated REE patterns of the fluid in equilibrium with the dioritic and granitic facies of the Traversella intrusion (see Table 2) (K_D from Flynn and Burnham 1978). The North American Shale Composite (Gromet et al. 1984) is given for the metamorphic and meteoric fluids

In conclusion, the REE geochemistry has shown that 1) the different types of skarn have very much the same type of distribution whatever the original rock and this suggests that the same type of fluid is responsible for all; 2) there is a strong input of REE during skarn formation; 3) this primary metasomatic fluid is characterized by a LREE fractionation and no observable Eu anomaly; 4) the REE data alone cannot be used here as discriminant parameters to trace the source of the fluid(s).

O – C isotopes

The calculated $\delta^{18}O$ of the metasomatic fluid (Table 6) in equilibrium ($T=600°$ C) with the primary skarn minerals ranges from 8.3 per mil to 8.95 per mil. This value is close to that calculated for the fluid in equilibrium with the diorite: +8.0 per mil at $T=750°$ C.

The $\delta^{13}C$ of the metasomatic fluid in equilibrium with the calcite no. 16 is – 5.4 per mil at the temperature of skarn formation ($T=600°$ C) (Friedman and O'Neil 1977). Any direct measure of $\delta^{13}C$ composition of the magma is not available, but this value is likely to be within the range of the mantle $\delta^{13}C$ (−5 per mil to −8 per mil: Taylor et al. 1967).

In conclusion, both $\delta^{18}O$ and $\delta^{13}C$ data indicate that the primary metasomatic fluid could have been in equilibrium with the diorite.

Table 6. $\delta^{18}O$ of the fluid in equilibrium with the primary skarn minerals and the diorite

Mineral	$\delta^{18}O$ mineral (per mil)	Mineral-fluid	$\delta^{18}O$ fluid (per mil)
1. *Skarns (early stage)*			
Calcite (16)	+9.7	O'Neil et al. (1969) $T=600°$ C	+8.95
Diopside (27)	+7.2	Matthews et al. (1983)	+8.3
Garnet (28)	+5.4	Taylor and O'Neil (1977)	+8.5
2. *Diorite*			
Plagioclase[a]	+7.2 to +7.8	O'Neil and Taylor (1967) Ohmoto (1986) $T=750°$ C	+8.0

[a] Data from van Marcke de Lummen and Vander Auwera (1990)

Sr isotopes evidence

The position of sample 33 in the range of fresh samples of the intrusion and sample 34 slightly above suggests that the fluid responsible for the late alteration of the intrusion (according to field observation, this event is later than the early stage of skarn development, but probably contemporaneous with the secondary stage of these skarns) has a similar I_{Sr} to that of the diorite or that this slight alteration has not affected the I_{Sr} of these two samples. The first hypothesis is likely in view of the comparable I_{Sr} of the epidote relative to the I_{Sr} of the fresh samples of intrusion. Because the oxygen isotopic composition of these samples 33 and 34 falls close to that of the primary magmatic rocks (van Marcke de Lummen and Vander Auwera 1990) a very small amount of O exchange with connate water is expected for these rocks. Therefore, their I_{Sr} is likely to be a primary magmatic feature (Criss and Fleck 1986). The relatively large range observed in the I_{Sr} of the dioritic samples has been attributed to an assimilation fractional crystallization process (AFC) (van Marcke de Lummen and Vander Auwera 1990). This dispersion implies that the $(^{87}Sr/^{86}Sr)_0$ of the fluid(s) in equilibrium with the diorite and assumed to be responsible for the skarn formation will also show a range of I_{Sr}. Otherwise, the magnitude of $^{87}Sr/^{86}Sr$ alterations depends strongly on the degree of Sr accommodation in the secondary minerals: epidote in particular is a good trap for the hydrothermal Sr (André and Deutsch 1986).

I_{Sr} and bulk Sr contents have distinct behavior in the two types of metasomatic columns developed in dolomitic marbles. In the case of the metasomatic wollastonite column where the Sr content is not leached (see earlier), the I_{Sr} of the skarn minerals remains within range of that of the dolomitic marbles. On the contrary, in the metasomatic garnet column, the Sr is leached in the internal part of the skarn (clinopyroxene) and the I_{Sr} increases from the dolomitic marble (calcite) values into the range of values for the intrusion clinopyroxene. This phenomenon does not seem to be induced by a mineralogical control. Indeed, although the pyroxenes of these two columns have the same composition, their bulk Sr content are clearly different (209 ppm Sr for the clinopyroxene of the wollastonite column and 31 ppm Sr for the clinopyroxene of the andradite-rich garnet column). This feature is better explained by a difference in water/rock (W/R) ratio: the $\delta^{18}O-\delta^{13}C$ of the calcite from the metasomatic wollastonite column indicates a much lower W/R than in the metasomatic andradite column (see later section). From these observations, at low W/R, the I_{Sr} of the skarn remains close to that observed in the dolomitic marbles and is therefore most probably inherited from those of the original rocks. Inversely, when the Sr is leached (high W/R) in the internal part of the metasomatic column (cpx) the I_{Sr} increases from the values for the dolomitic marbles recorded in the calcite up to the values for the intrusion recorded in the clinopyroxene. In the case of the skarns developed in gneisses and in calcic hornfelses, the I_{Sr} of the original rock (gneiss or calcic hornfels) is not available but we can observe for example that the minerals and garnet have also an I_{Sr} within the range of values for the intrusion,

To summarize, as with the stable isotopes, the Sr isotopes thus point to a primary metasomatic fluid equilibrated with the intrusion. Moreover, the Sr isotopic composition observed in the skarn minerals results from a mixing process between the original rock I_{Sr} and that from the fluid both weighted by their respective proportions of Sr.

Modeling of $\delta^{13}C-\delta^{18}O$ depletion during skarn formation and evaluation of the water-rock ratios (W/R)

The isotopic data (Fig. 4) imply that the metasomatic transformation of the marbles induces a sharp and continuous decrease in $\delta^{18}O$ together with a gradual but smaller decrease in $\delta^{13}C$. Moreover, even the dolomitic marbles near the skarns have been depleted in $\delta^{18}O-\delta^{13}C$. In view of the clustering of values in unmodified marbles, it seems reasonable to average the values at $\delta^{18}O=+21.6$ per mil and $\delta^{13}C=-0.93$ per mil (named reference value on Fig. 4).

This depletion in $\delta^{18}O$ and $\delta^{13}C$ of skarn calcites, a well known phenomenon in other skarn deposits (Taylor and O'Neil 1977; Guy 1979; Bowman et al. 1985; Taylor and Bucher-Nurminen 1986), can be assigned either to the marble decarbonation during skarn formation (Shieh and Taylor 1969) or to the equilibration of the isotopic composition of the rock with that of the H_2O-rich metasomatic fluid (Bowman et al. 1985; Taylor and Bucher-Nurminen 1986). Guy et al. (1988) have also suggested that $\delta^{18}O$ and $\delta^{13}C$ are not coupled during the skarn formation process. According to their magmatic hydrothermal model, the $\delta^{18}O$ of the skarn calcites is controlled by the interaction with the infiltrating fluid and the $\delta^{13}C$, by the decarbonation reaction. The first two models will be discussed in turn.

Decarbonation reaction. Within the temperature range of the early skarn formation (T=550° C to 625° C, see earlier) the CO_2-calcite isotopic fractionation is such that the CO_2 produced by the decarbonation is enriched in both $\delta^{18}O$ and $\delta^{13}C$ relative to the calcite [(using the fractionation factor of Bottinga (1968))]. In the present case, decarbonation is described by the following reaction:

$$CaMg(CO_3)_2 + 1/2(SiO_2)_{aq.} = 1/2\,Mg_2SiO_4 + CaCO_3 + CO_2 \quad (1)$$
dolomite fluid forsterite calcite

in which the required SiO_2 is provided by the metasomatic fluid. In order to restrict the test to the effect of the decarbonation, the isotopic composition of the oxygen present in SiO_2 has not been considered. An open-system decarbonation process has been considered here because it is more likely to have operated in the development of infiltration skarn. The results of the calculations are plotted on Fig. 8 (see Appendix for detail). The initial isotopic composition of the dolomitic marble (figured as a star on Fig. 4) has been taken as the mean isotopic composition of the marbles located outside the contact aureole. Figure 8 suggests that the process is not efficient enough to explain the observed depletion in the primary skarn calcite. This can be due to the fact that in the transformation of the marble into an assemblage of forsterite + calcite, half the carbon orginally present in the dolomite is conserved within the skarn calcite while two-thirds of the original oxygen is preserved within the forsterite and the calcite. The effect of decarbonation on the oxygen and carbon isotopic composition are thus concluded to be of minor importance. This result is in agreement with the conclusion of Bowman et al. (1985) and Taylor and Bücher-Nurminen (1986).

Interaction with infiltrating fluid. The isotopic variations observed in the skarns developed on dolomitic marbles can result from various mixtures between the unmodified dolomitic marble ($\delta^{18}O = +21.6$ and $\delta^{13}C = -0.93$ per mil) and an infiltrating metasomatic fluid. Since the isotopic data suggest that this fluid could have been in equilibrium with the nearby cooling diorite, we have selected for the metasomatic fluid the $\delta^{18}O$ of the fluid calculated in equilibrium with diorite, i.e., 8.0 per mil (see earlier). The $\delta^{13}C$ of this fluid can be estimated to vary within those values measured in magmatic rocks from −2.5 per mil to −32.5 per mil (Javoy et al. 1986). Because of this relatively wide range of values, we have calculated the model for several discrete $\delta^{13}C$ values ($\delta^{13}C = -5$ per mil; −8 per mil; −15 per mil; −20 per mil). Since the primary stage of skarn formation is likely to be isothermal, the calcite isotopic composition is mainly controlled by the water/rock ratio (W/R) [(atomic fraction of oxygen or carbon present in the fluid relative to the atomic fraction of oxygen or carbon present in the rock (Taylor 1977)]. In an open system, each small batch of pore-filling fluid equilibrates with the rock and then moves out [single-pass model, Taylor (1974)]; the system is then refilled by a fluid of the same initial isotopic composition. In other words, the fluid isotopic composition is externally controlled (Taylor and Bücher-Nurminen 1986). Such an open system behavior is assumed here because it is relevant for the development of infiltration skarn (Korzhinskii 1970; Fonteilles personal communication). The model was calculated for different isotopic compositions ($\delta^{13}C$) of the metasomatic fluid (Fig. 8) [after Taylor and Bucher-Nurminen (1986)] (see Appendix). A decrease of fluid $\delta^{13}C$ progressively reduces the concavity of the theoretical curve. An increase of X_{CO_2} has the same effect as that observed with the $\delta^{13}C = -5$ per mil curve which has been calculated for two values of X_{CO_2} (0.05 and 0.1 compatible with the mineral parageneses developed during the primary stage (Vander Auwera 1988)). Comparison of the observed curve with the theoretical curves (Fig. 8) suggests that: 1) this model is able to induce the observed hyperbolic gradual depletion in $\delta^{13}C$ and $\delta^{18}O$; 2) the scattering

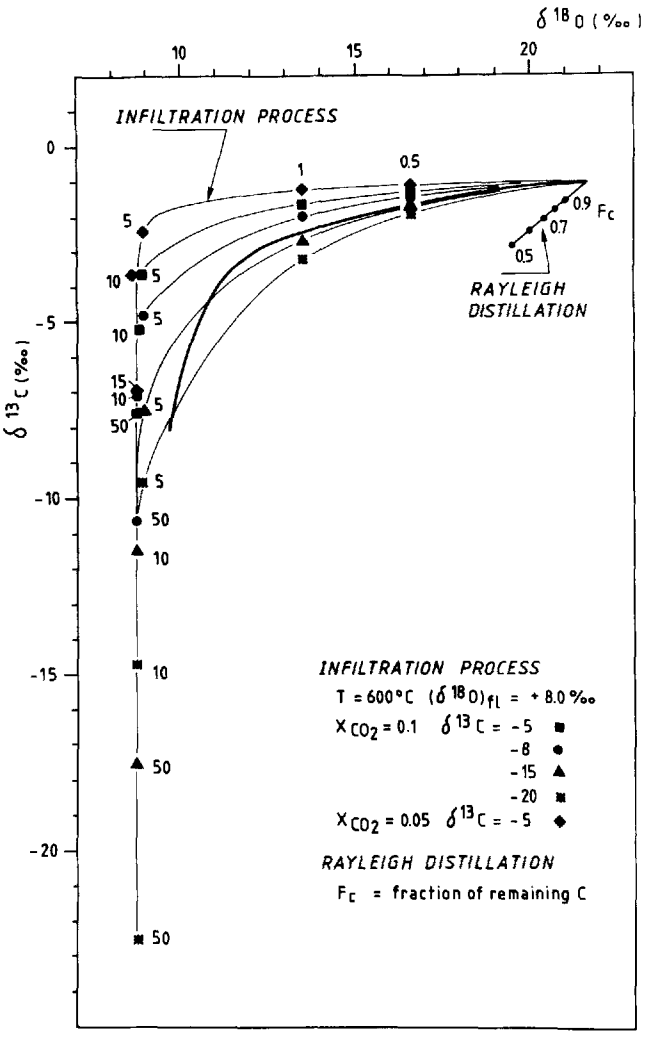

Fig. 8. Infiltration process and Rayleigh distillation modeling. For the infiltration process, several values of the $\delta^{13}C$ of the infiltrating fluid have been considered, with $X_{CO_2}=0.1$. In the case of $\delta^{13}C=-5$ per mil, an additional curve with $X_{CO_2}=0.05$ is shown. Numbers on the curves represent increasing W/R ratios. For the Rayleigh distillation model the *numbers* correspond to the fraction of C remaining in the rock (F_C). The *thick line* corresponds to the observed curve (see Fig. 4)

observed for the isotopic composition of the marbles located in the contact aureole is due to differences in W/R ratio and in initial isotopic composition; 3) the infiltration model permits a constraint of the W/R ratios prevailing during the skarn formation process. In the andradite column, W/R is probably between 10 and 50 whereas in the wollastonite column, it is only around 5–10. These W/R are usual values for skarn (Bowman et al. 1985; Taylor and Bucher-Nurminen 1986)

Source of the secondary fluid

O isotopes evidence

In Fig. 9, the isotopic composition of the fluid in equilibrium with the secondary minerals (amphibole, magnetite, calcite, chlorite, dolomite, scheelite) has been calculated for several temperatures within the determined temperature range (500° C to 300° C) using calibration values taken from the literature (Table 7). In Fig. 9, these values are plotted against the order of appearance of these secondary minerals (as deduced from Fig. 2).

At the onset of the first hydroxylation stage, there

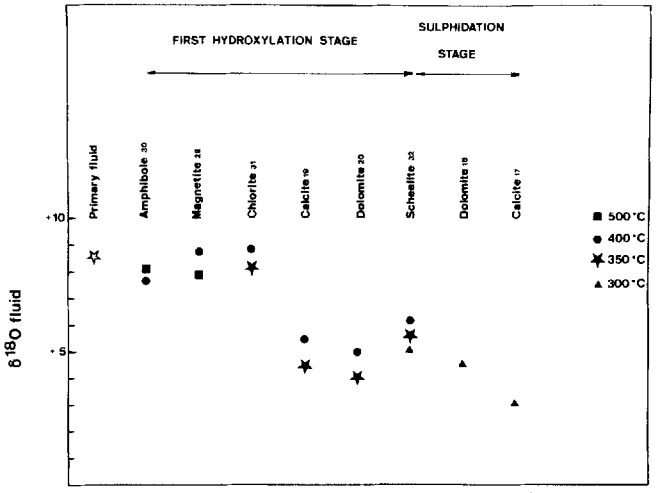

Fig. 9. $\delta^{18}O$ composition of the fluid in equilibrium with the secondary minerals at different temperatures (amphibole, magnetite, chlorite, calcite, dolomite for the first hydroxylation stage and scheelite, dolomite, calcite for the sulphidation stage, see Table 3). The isotopic composition of the primary fluid (see text) has been plotted for comparison

Table 7. Stable isotope fractionation factors

1) Calcite: CO_2-calcite ($\delta^{18}O$, $\delta^{13}C$): Bottinga (1968)
   H_2O-calcite ($\delta^{18}O$): O'Neil et al. (1969)
2) Dolomite: H_2O-dolomite ($\delta^{18}O$): Northrop and Clayton (1966)
3) Calcite-dolomite: ($\delta^{18}O$, $\delta^{13}C$): Sheppard and Schwarz (1970)
4) Scheelite-H_2O: ($\delta^{18}O$): Wesolowski and Ohmoto (1986)
5) Chlorite-H_2O ($\delta^{18}O$): Taylor (1979)
6) Magnetite-H_2O ($\delta^{18}O$): Becker and Clayton (1976)
7) Feldspar-amphibole ($\delta^{18}O$): Bottinga and Javoy (1974)
8) Diopside-H_2O ($\delta^{18}O$): Matthews et al. (1983)
10) Feldspar-olivine ($\delta^{18}O$): Bottinga and Javoy (1974)

is no significant change in $\delta^{18}O$ of the fluid in comparison with that observed in the primary stage fluid. In contrast, within the first hydroxylation stage, a sharp decrease in $\delta^{18}O$ is observed. Since both magnetite and calcite are end-members of H_2O-free solid solutions, this sharp decrease is not dependent upon the H_2O-mineral $\delta^{18}O$ calibration curve used for the calculation. Nor is it influenced by the temperature since we have considered a wide temperature interval for each mineral. It may be due to the arrival of another fluid with different isotopic characteristics or to a variation in the salinity of the same fluid (Ohmoto 1986). For the moment, no experimental data are available to control this last parameter. It may be considered that the occurrence of these two groups of isotopic data reflects a change in the fluid composition whatever the mechanism. Moreover, it is important to emphasize that all these minerals do not come from the same sample nor the same zone of the skarn. For example, amphibole developed at the expense of the diopside in the second zone of the skarn in dolomitic marbles and magnetite, at the expense of calcite of the first zone of these skarns. According to this observation, the isotopic composition of the fluid seems to be homogeneous during one particular step.

Such a sharp decrease in the secondary fluid $\delta^{18}O$ has not been observed in other skarn deposits where sufficient data are available. For example, in Elkhorn skarns (Bowman et al. 1985), $\delta^{18}O$ of the fluid decreases progressively from 11 per mil during the early stage to 5.5 per mil in the late hydrothermal one.

The decrease of the fluid $\delta^{18}O$ from 8.0 per mil to 3.0 per mil (Fig. 9) has been attributed, in other skarn deposits to mixing with meteoric fluid (Taylor and O'Neil 1977; Bowman et al. 1985). A rough estimate of the meteoric fluid $\delta^{18}O$ can be made here utilizing the data on the δD of the meteoric fluids during the Tertiary (Sheppard et al. 1969), at the latitude of Traversella (30° N during the Oligocene, after Smith and Briden 1977) ($\delta D = -30$ per mil) and using Craig's equation (1961). This evaluation gives a $\delta^{18}O = -5$ per mil. Mixing with meteoric water during the secondary stage can thus also account for the observed sharp decrease in the fluid $\delta^{18}O$. The jump observed for the $\delta^{18}O$ variation between the early ($\delta^{18}O = +8.0$ per mil) and the late ($\delta^{18}O = +5.0$ per mil) sections of the first hydroxylation stage (Fig. 9) implies a rapid change in the fluid dynamics between the crystallization of the magnetite and the scheelite.

During the sulphidation stage, the smooth $\delta^{18}O$ evolution can also be interpreted as due to a similar but more progressive mixing.

Sr isotopes evidence

The strong enrichment in ^{87}Sr observed in the secondary minerals (Fig. 6) can be due to the interaction with: 1) a fluid equilibrated with a high I_{Sr} facies of the intrusion; 2) a meteoric fluid; 3) a meteoric fluid equilibrated with the country rocks. The first hypothesis cannot explain the very high I_{Sr} at the end of the sulphidation stage.

Due to its very low Sr concentration, the pristine meteoric water is also unlikely to modify significantly the I_{Sr} of the Sr-rich forsterite-calcite zone of the skarns through which it percolates, unless an improbably high W/R ratio is assumed. In contrast, the Sr isotopic composition of the meteoric fluid can be modified according to the stability of the mineralogical phase of the country rocks through which it percolates. So the destabilization of a Rb-rich mineral (for example, the abundant biotite of the surrounding gneisses) can produce ^{87}Sr-enriched fluid that can readily change the I_{Sr} of the secondary mineral phases. It is not possible to determine whether, the increase in I_{Sr} during the sulphidation stage is due to an increase in the W/R ratio, or to a modification in the nature of the destabilized Rb-rich phase. However, the combined stable and radiogenic isotope data put some constraints on the timing of the ore deposition (essentially magnetite and scheelite): 1) during the precipitation of magnetite the fluid had always the same O – Sr isotopic signatures as in the early stage; 2) according to both $\delta^{18}O$ and I_{Sr} data, the scheelite crystallization coincides with a large increase in the proportion of the meteoric water in the metasomatic fluid. This suggests that the precipitation of scheelite could be related to the mixing process between the "magmatic-derived" fluids and the "meteoric-derived" fluids. Indeed, this can induce a significant variation in the controlling factors (temperature, salinity, pH) of the scheelite solubility (Eugster 1985).

Conclusions

This geochemical study emphasizes the value of using several independant parameters to trace the origin of the skarn ore bodies: 1) the REE patterns suggest that the different types of skarn result from the interaction between the same fluid and several types of orginal rocks; 2) the modeling of the stable isotopes behavior ($\delta^{13}C$, $\delta^{18}O$) in skarns developed in dolomitic marbles can be used to deduce some information on the W/R ratio that characterizes this interaction; 3) the determinant parameter controlling the repartition of trace elements between fluid and rock seems to be the W/R ratio and not the equilibrium distribution factor; 4) the comparison of the I_{Sr} data (deduced from the Sr-rich minerals) with the $\delta^{18}O$ values is very useful to constrain the variations of the fluid dynamics in response to decreasing temperature.

The following model is suggested for the Traversella skarn deposit. During the primary stage, a fluid isotopically ($\delta^{18}O$, $^{87}Sr/^{86}Sr$) in equilibrium with the intrusion percolated through the surrounding rocks of the intrusion and was responsible for the development of the primary metasomatic columns by infiltration metasomatism. This primary fluid was either a magmatic fluid exsolved from the crystallizing magma, or a metamorphic fluid equilibrated with the intrusion near its solidus temperature.

At the beginning of the first hydroxylation stage of the skarn evolution, there was no significant change in the isotopic composition of the fluid. This stage, characterized by the precipitation of magnetite, corresponds to the stabilization of hydrated phases in response to decreasing temperature. At the end of the first hydroxylation stage, temperature has further decreased and the intrusion has completely crystallized. A meteoric fluid, possibly involved in a convective circulation centered on the intrusion, quickly penetrated the system and mixed with the primary fluid. This mixture could be the cause of the precipitation of the scheelite in the late stage of the hydroxylation process.

Appendix

Open system decarbonation. – In this case, the CO_2 produced is immediately expelled from the rock, the process can be modelled by a Rayleigh distillation equation (Rumble III 1982; Bowman et al. 1985):
$\delta^{13}C_f = (\delta^{13}C_i + 1000) f^{\alpha_{CO_2\text{-rock}}-1} - 1000$ in which $\delta^{13}C_i$, represents the initial isotopic composition of the carbon in the rock; $\delta^{13}C_f$, the final isotopic composition of the rock; f, the atomic fraction of C remaining in the rock and $\alpha_{CO_2\text{-rock}}$ is the fractionation factor of the $^{13}C/^{12}C$ between the CO_2 and rock. A similar equation can be written for $\delta^{18}O$. The calculation gives the final isotopic composition of the rock after each increment of the reaction. At each step, the mineral proportions are different and the value of the parameter $\alpha_{CO_2\text{-rock}}$ changes. This parameter can be calculated using the Rumble III (1982) equation.

Infiltration process. – In an open system, the isotopic changes of the calcite induced by the H_2O-rich metasomatic fluid can be calculated by a mass balance equation (Taylor 1974; Taylor and Bucher-Nurminen 1986). For $\delta^{18}O$, the reaction is:

$$W/R = 1n \frac{(\delta^{18}O_{H_2O})_i + (\Delta - (\delta^{18}O_{cc})_i)}{(\delta^{18}O_{H_2O})_i - ((\delta^{18}O_{cc})_f - \Delta)}$$

where Δ is the water-calcite oxygen isotopic fractionation factor; i = initial; f = final and W/R is the water to rock atom mass ratio. A similar equation is used to describe carbon isotope exchange, taking into account the concentration of carbon in the fluid (Taylor and Bucher-Nurminen 1986);

$$X_{CO_2} \cdot W/R = \ln \frac{(\delta^{13}C_{CO_2})_i + (\Delta - (\delta^{13}C_{cc})_i)}{(\delta^{13}C_{CO_2})_i - ((\delta^{13}C_{cc})_f - \Delta)}$$

in which Δ represents the calcite-CO_2 carbon isotope fractionation factor.

Acknowledgements. Stable isotopes analyses of carbonates and REE of three samples were kindly carried out by Dr. G. van Marcke de Lummen (Stable Isotope Laboratory of Utrecht) and Dr. T. Williams (British Museum: Natural History, London), respectively. The helpful comments of Prof. J.C. Duchesne (University of Liège), Prof. P. Henderson (British Museum: Natural History) and Prof. J. Touret (Vrije Universiteit: Amsterdam) are gratefully acknowledged. V. Miocque (University of Liège) provided technical assistance. This research is part of a PhD thesis (Vander Auwera J) funded by an IRSIA fellowship and partly supported by an EEC contract.

References

Andre L, Deutsch S (1986) Magmatic $^{87}Sr/^{86}Sr$ relicts in hydrothermally altered quartz diorites (Brabant Massif, Belgium) and the role of epidote as a Sr filter. Contrib Mineral Petrol 92:104–112

Becker RH, Clayton JRN (1976) Oxygen isotope study of a precambrian banded iron-formation. Hamersley Range, Western Australia. Geoch Cosmochim Acta 40:1153–1165

Böhlke JK, Kistler RW (1986) Rb–Sr, K–Ar and stable isotope evidence for the ages and sources of fluid components of gold-bearing quartz veins in the Northern Sierra Nevada, Foothills, Metamorphic Belts, California. Econ Geol 81:296–322

Bottinga Y (1968) Calculation of fractionation factors for carbon and oxygen exchange in the system calcite-carbon dioxide-water. J Phys Chem 72:800–808

Bottinga Y, Javoy M (1974) Oxygen isotope geothermometry of igneous and metamorphic rocks. EOS 55:477

Bowman JR, O'Neil JR, Essene EJ (1985) Contact skarn formation at Elkhorn, Montana. II: Origin and evolution of C–O–H skarn fluids. Am J Sci 285:621–660

Burt DM (1972) Mineralogy and geochemistry of Ca–Fe–Si skarn deposits. PhD Thesis, Harvard University

Burt DM (1977) Mineralogy and petrology of skarn deposits. Rend Soc It Min e Pet 33(2):859–873

Changkakoti A, Ghosh DK, Krstic D, Gray J, Morton RD (1986) Pb and Sr isotope compositions of hydrothermal minerals from the Great Bear Lake Silver deposits, N.W.T., Canada. Econ Geol 81:739–743

Chessex R (1962) Détermination d'âge de quelques roches des Alpes du Sud par la "méthode des dommages dus à la radioactivité". Schweiz Mineral Petrogr Mitt 42:652–654

Colomba L (1913) Ricerche sui giacimenti di Brosso e di Traversella Parte prima. Osservationi petrografische sul massicio dioritico di Valchiusella. Memorie della R Accad delle Scienze di Torino. Serie seconda. Sci Fis Mat Nat 63:271–325

Craig H (1961) Isotopic variations in meteoric waters. Science 133:1701–1703

Criss RE, Fleck RJ (1986) Petrogenesis, geochronology and hydrothermal systems of the nothern Idaho batholith region based on $^{18}O/^{16}O$, D/H, $^{87}Sr/^{86}Sr$, K–Ar and $^{40}Ar/^{39}Ar$ studies. US Geol Surv Prof Pap 1436

Cullers RL, Medaris LG, Haskin LA (1973) Experimental studies of the distribution of rare earths as trace elements among silicate minerals and liquids and water. Geochim Cosmochim Acta 37(6):1499–1512

Debelmas J, Lemoine M (1970) The western Alps: palaeogeography and structure. Earth Sci Rev 6:221–256

Dubru M, Vander Auwera J, Van Marcke de Lummen (1988) Distribution of Scheelite in magnesian skarns at Traversella (Piemontese Alps, Italy) and Costabonne (Eastern Pyrenées; France): Nature of the associated magmatism and influence of fluid composition. SGA Special publications, vol 6. Springer, Berlin Heidelberg New York, pp 117–134

Einaudi MT, Meinert LD, Newberry RJ (1981) Skarn deposits. Econ Geol 75th anniversary volume:317–391

Eugster HP (1985) Granites and hydrothermal ore deposits: a geochemical framework. Min Mag 49:7–23

Flynn RT, Burnham CW (1978) An experimental determination of rare-earth partition coefficients between a chloride containing vapor phase and silicate melts. Geochim Cosmochim Acta 42:685–701

Fonteilles M (1978) Les mécanismes de la métasomatose. Bull Minéral 101:166–194

Fourcade S (1981) Géochimie des granitoïdes. Thesis University of Paris

Friedman I, O'Neil J (1977) Compilation of stable isotope fractionation factors of geochemical interest in: Data of geochemistry M. Fleischer (ed) Geol Surv Prof Pap, m440–KK

Govindaraju K, Mevelle G (1987) Fully automated dissolution and separation methods for inductively coupled plasma atomic emission spectrometry rock analysis. Application to the determination of REE. J Anal Atom Spectrom 2:615–621

Gresens RL (1967) Composition – Volume relatioships of metasomatism. Chem Geol 2:47–65

Gromet LP, Dymek RF, Haskin LA, Korotev RL (1984) The North American Shale composite: Its compilation, major and trace element characteristics. Geochim Cosmochim Acta 48:2469–2482

Guy B (1979) Pétrologie et géochimie isotopique (S, C, O) des skarns à scheelite de Costabonne, Pyrénées orientales. Thèse, ENSM Paris

Guy B, Sheppard SMF, Fouillac AM, Le Guyader R, Toulhoat P, Fonteilles M (1988) Geochemical and isotopic studies of barren and tungsten-bearing skarns of the French Pyrenées. In: Mineral Deposits within the European Community. Boissonas J and Omenetto P (eds), Springer, Berlin Heidelberg New York Tokyo, 53–75

Henderson P (1984) General geochemical properties and abundances of the rare-earth elements. In: Henderson (ed) Rare earth element geochemistry, Elsevier, Amsterdam

Hoefs J (1980) Stable isotope geochemistry, 2nd edn. Springer, Berlin Heidelberg New York

Hofmann A (1972) Chromatographic theory of infiltration metasomatism and its application to feldspars. Am J Sci 271:69–90

Hunziker JC (1974) Rb–Sr and K–Ar age determination and the alpine tectonic history of the western Alps. Mem Ist Geol Min Univ Padova 31:1–55

Javoy M, Pineau F, Delorme H (1986) Carbon and Nitrogen isotopes in the mantle. Chem Geol 57:41–62

Kennedy WQ (1931) The igneous rocks, pyrometasomatism and ore deposition at Traversella Piedmont, Italy. Schweiz Mineral Petrogr Mitt:77–138

Korzhinskii DS (1970) The theory of metasomatic zoning. Clarendon Press, Oxford

Krummenacher D, Evernden JF (1960) Détermination d'âge isotopique sur quelques roches des Alpes par la méthode K–Ar. Schweiz Mineral Petrogr Mitt 40:267–277

Martin JM, Hogdahl O, Philipott SC (1976) Rare earth element supply to the ocean. J Geophys Res 81:3119–3124

Matthews A, Goldsmith JR, Clayton RN (1983) Oxygen isotope fractionation including pyroxenes: the calibration of mineral pair geothermometer. Geochim Cosmochim Acta 17:631–644

Müller F (1912) Die Erzlagerstatten von Traversella im Piedmont, Italien. Zeitschr für Prakt Geol 20:209–240

Nord AG, Billström K (1982) A system for stable isotope analyses of geological samples. Geol Fören Stockholm Förh 104:113–120

Norman DI, Landis GP (1983) Source of mineralizing components in hydrothermal ore fluids as evidence by $^{87}Sr/^{86}Sr$ and stable isotope data from the Pasto Bueno deposit, Peru. Econ Geol 78:451–465

Northrop DA, Clayton JRN (1966) Oxygen isotope fractionations in system containing dolomite. Jour Geol 74:174–196

Novarese V (1943) Il sistema eruttivo Traversella-Biella. R. Ufficio Geol, Roma

Ohmoto (1986) Stable isotope geochemistry of ore deposits. In: Reviews in Mineralogy, no 16: Stable Isotopes in High Temperature Geological Processes, Valley JW, Taylor HP, O'Neil JR (eds), Min Soc Amer 16:491–560

O'Neil JR, Clayton RN, Mayeda TK (1969) Oxygen isotope fractionation in divalent metal carbonates. J Chem Phys 51:5547–5558

O'Neil JR, Taylor HP Jr (1967) The oxygen isotope and cation exchange chemistry of feldspars. Am Mineral 52:1414–1437

Rumble D III (1982) Stable isotope fractionation during metamorphic devolatilization reactions. In: Reviews in Mineralogy no 10: Characterization of metamorphism through mineral equilibria. Ferry JM (ed), Min Soc Amer 10:327–352

Sheppard SMF, Nielsen RL, Taylor HP (1969) Oxygen and hydrogen isotope ratios of clay minerals from porphyry copper deposits. Econ Geol 64:755–777

Sheppard SMF, Schwarcz HP (1970) Fractionation of carbon and oxygen isotopes and magnesium between metamorphic calcite and dolomite. Contrib Mineral Petrol 26:161–198

Shieh YN, Taylor HP (1969) O and C isotope studies of contact metamorphism of carbonate rocks. J Petrol 10:307–331

Smith AG, Briden JC (1977) Mesozoic and cenozoic paleocontinental maps. Cambridge Earth Science Series, Cambridge

Taylor HP (1974) The application of oxygen and hydrogen isotope studies to problems of hydrothermal alteration and ore deposition. Econ Geol 69:843–883

Taylor HP (1977) Water/Rock interaction and the origin of H_2O in granitic batholits. J Geol Soc London 133:509–558

Taylor HP (1979) Oxygen and hydrogen isotope relationships in hydrothermal deposits. In: Barnes HL (ed) Geochemistry of hydrothermal deposits, Wiley, pp 236–277

Taylor HP, Frechen J, Degens ET (1967) Oxygen and carbon isotope studies of carbonatites from the Laacher See district, West Germany and the Alno-district, Sweden. Geochim Cosmochim Acta 31:407–430

Taylor BE, O'Neil JR (1977) Stable isotope studies of metasomatic Ca–Fe–Al–Si skarns and associated metamorphic and igneous rocks, Osgood mountains, Nevada. Contrib Mineral Petrol 63:1–49

Taylor BE, Bücher-Nurminen K (1986) Oxygen and carbon isotope and cation geochemistry of metasomatic carbonates and fluids. Bergell aureole, northern Italy. Geochim Cosmochim Acta 50:1267–1279

Trümpy R (1960) Paleotectonic evolution of the central and western Alps. Bull Geol Soc Am 71:843–908

Vander Auwera J (1988) Pétrologie et géochimie (terres rares, $^{18}O/^{16}O$, $^{13}C/^{12}C$, $^{87}Sr/^{86}Sr$) des skarns ferrifères et tungstifères de Traversella (Ivrea, Italie). Thèse University Catholic Louvain

Vander Auwera J (1990) The porphyritic facies and the endoskarns of the Traversella monzodiorite: implications for the evolution of the main intrusion. Schweiz Mineral Petrol Mitt 2/70 (in press)

van Marcke de Lummen G, Vander Auwera J (1990) Petrogenesis of the Traversella diorite (Piemonte, Italy): a major and trace elements and isotopic (O, Sr) modelling. Lithos 24:121–136

Wesolowski D, Ohmoto H (1986) Calculated oxygen isotope fractionation factors between water and the minerals scheelite and powellite. Econ Geol 81:471–477

Wirth R (1985) Dehydration of mica (phengite) by electron bombardment in a transmission electron microscope (TEM). J Mat Sci Lett 4:327–330

Wirth R (1986) Thermal alteration of glaucophane in the contact aureole of the Traversella intrusion (North Italy). Neues Jahrb Mineral Abb 154(2):193–205

Editorial Responsibility: J. Touret